Volume 10 | Number 19 | 21 May 2019 | Pages 4933–5186

Chemical Science

rsc.li/chemical-science

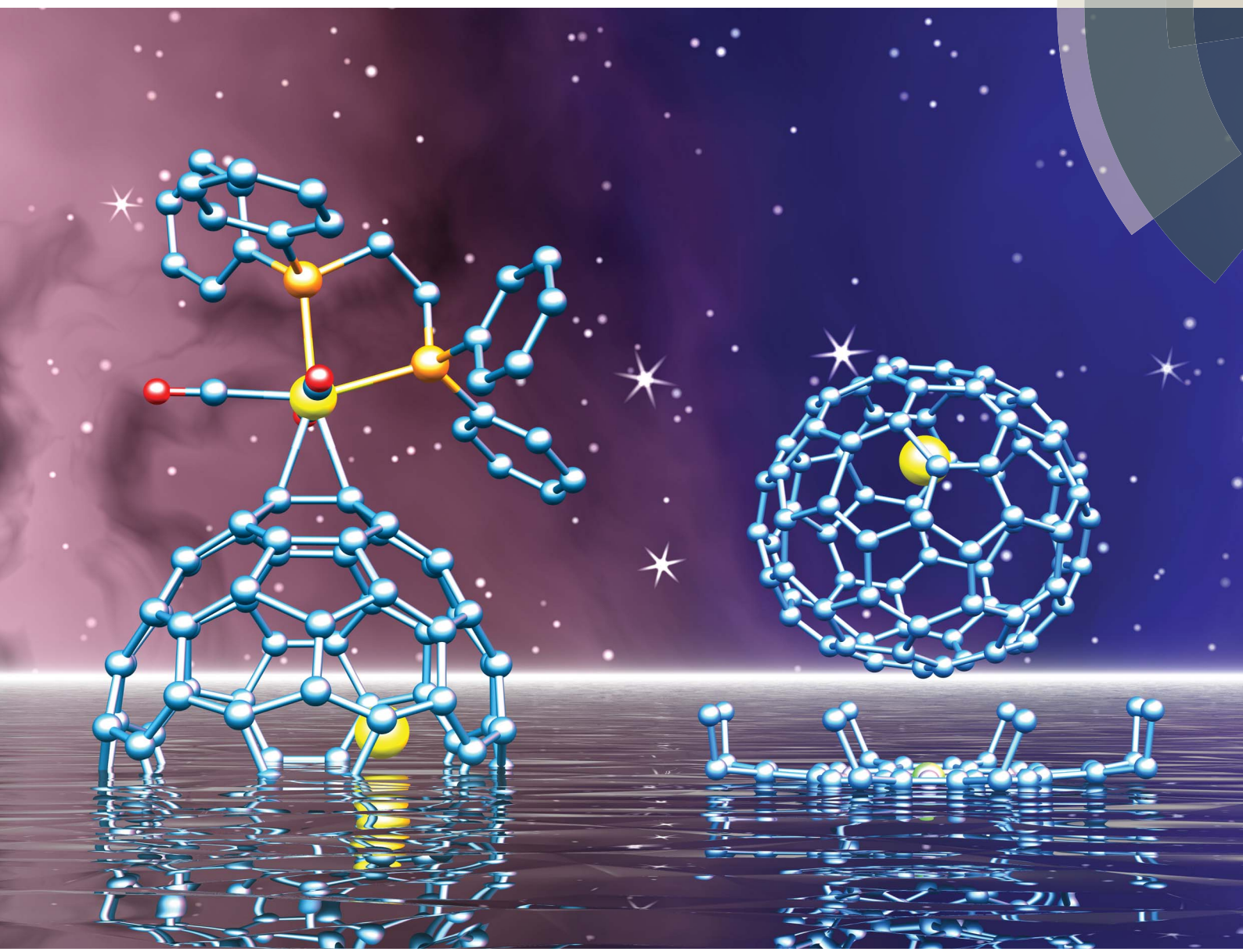

ISSN 2041-6539

ROYAL SOCIETY OF CHEMISTRY | Celebrating IYPT 2019

EDGE ARTICLE

Peng Jin, Shuquan Liang, Xing Lu *et al.*

Highly regioselective complexation of tungsten with Eu@C_{82}/Eu@C_{84}: interplay between endohedral and exohedral metallic units induced by electron transfer

Chemical Science

EDGE ARTICLE

View Article Online
View Journal | View Issue

Cite this: *Chem. Sci.*, 2019, **10**, 4945

All publication charges for this article have been paid for by the Royal Society of Chemistry

Highly regioselective complexation of tungsten with Eu@C_{82}/Eu@C_{84}: interplay between endohedral and exohedral metallic units induced by electron transfer†

Lipiao Bao,[a] Pengyuan Yu,[a] Ying Li,[b] Changwang Pan,[a] Wangqiang Shen,[a] Peng Jin,*[b] Shuquan Liang*[c] and Xing Lu*[a]

Interactions between the inner and outer units through a fullerene cage are of fundamental importance for the creation of molecular spintronics and machines, but the mechanism of such through-cage interplay is still unclear. In this work, we have designed and synthesized two prototypical compounds which contain only a single europium atom inside the cage and merely a tungsten atom coordinating outside to clarify the interactions between the endohedral and exohedral metallic units. They are obtained by reacting a tungsten complex $W(CO)_4(Ph_2PC_2H_4PPh_2)$ (**1**) with the corresponding metallofullerenes in a highly regioselective manner (**2a** for Eu@C_2(5)-C_{82} and **2b** for Eu@C_2(13)-C_{84}). On the one hand, the endohedral Eu-doping has changed the LUMO distribution on C_2(5)-C_{82}/C_2(13)-C_{84} dramatically, *via* electron transfer, which governs the addition pattern of the exohedral tungsten resulting in surprisingly high regioselectivity. On the other hand, the exohedral tungsten coordination with Eu@C_2(5)-C_{82}/Eu@C_2(13)-C_{84} has restricted the motion of the internal europium ion to some extent by changing the electrostatic potentials, as confirmed by the X-ray results of **2a**, **2b** and the corresponding pristine metallofullerenes cocrystallized with Ni(OEP) (OEP is the dianion of octaethylporphyrin). We now make it clear that the interplay between the endohedral and exohedral metallic units can be realized in a single system by means of intramolecular charge transfer, which may arouse interest in the design and utilization of novel metallofullerene-based molecular devices.

Received 26th March 2019
Accepted 25th April 2019

DOI: 10.1039/c9sc01479a

rsc.li/chemical-science

Introduction

Confining metal atom(s) or metallic units inside fullerene cages affords a collection of novel hybrid molecules named endohedral metallofullerenes (EMFs).[1–6] Results show that the internal metallic units are able to influence the chemical properties of the cage carbon atoms through, for example, charge transfer and/or the geometric effect. For instance, Sc_2C_2-doping of D_{2d}(23)-C_{84} altered its chemical reactivity dramatically by raising the HOMO and LUMO levels so that D_{2d}(23)-C_{84} and Sc_2C_2@D_{2d}(23)-C_{84} follow different routes when reacting with 2-adamantane-2,3′-[3*H*]-diazirine.[7] Besides, the size effect of the internal cluster has been observed in the 1,3-dipolar reactions of M_3N@I_h-C_{80} (M = Sc, Y, Er and Gd) where EMFs with a small M_3N cluster (M = Sc and Y) give [5,6]-adducts but that containing a larger Gd_3N or Er_3N cluster favors the formation of [6,6]-adducts.[8–11]

On the other hand, the impact of the external addition on the position and even the configuration of the internal metallic units has also been demonstrated. Systematic studies of Akasaka and coworkers evidenced that the dynamic behavior of the encaged metal atoms in M_2@I_h-C_{80} (M = Ce and La) is drastically restrained upon chemical functionalization of the cage mainly by geometric distortion.[12] Recently, a collaborative study demonstrated that the attachment of a benzyl radical on Sc_3C_2@C_{80} alters the configuration of the internal Sc_3C_2 cluster from a bat-ray-like shape to a trifoliate one[13] whereas another brilliant study reported that the magnetic properties of Sc_3C_2@C_{80} can also be altered by attaching a remote nitroxide radical.[14]

Even though the impact from the outer on the inner moieties or the reverse process has been clearly demonstrated, it is still blurry whether the endohedral–exohedral interactions can be realized simultaneously in a single system. In their pioneering work, Popov and coworkers reported that the addition of 14 or 16 CF_3 groups onto Sc_3N@C_{80} confines the geometry of the

[a]*State Key Laboratory of Materials Processing and Die & Mould Technology, School of Materials Science and Engineering, Huazhong University of Science and Technology, 1037 Luoyu Road, Wuhan, 430074, China. E-mail: lux@hust.edu.cn*

[b]*School of Materials Science and Engineering, Hebei University of Technology, Tianjin, 300130, China. E-mail: china.peng.jin@gmail.com*

[c]*Department of Materials Science and Engineering, Central South University, Changsha, 410083, China. E-mail: lsq@csu.edu.cn*

† Electronic supplementary information (ESI) available: HPLC profiles and theoretical calculation results. CCDC 1579794, 1579799, 1579800 and 1851767. For ESI and crystallographic data in CIF or other electronic format see DOI: 10.1039/c9sc01479a

internal Sc_3N cluster and the multi-addition pattern seems to be a result of cluster–cage interactions.[15] Similar results were also obtained in the YCN@$C_{84}(CF_3)_n$ (n = 16 and 18) system recently.[16] However, because of the existence of multiple endohedral atoms and many exohedral addends in these examples, it is still difficult to clarify the fundamental mechanism of the endohedral–exohedral interactions.

Herein, we have synthesized two coordination complexes (**2a** and **2b**) by reacting a tungsten complex $W(CO)_4(Ph_2PC_2H_4PPh_2)$ (**1**) with either Eu@$C_2(5)$-C_{82} or Eu@$C_2(13)$-C_{84}. **2a** and **2b** are ideal prototypes for understanding through-cage interactions because only one europium atom is encapsulated inside the cage with merely a tungsten atom coordinating outside. Based on the concrete crystallographic and theoretical results, the interactions between the inner and outer metallic units have been well documented for the first time by considering intramolecular charge transfer as the main driving force.

Results and discussion

Chemical functionalization of Eu@C_{82}/Eu@C_{84}

Photo-irradiation of a toluene solution containing Eu@$C_2(5)$-C_{82} and $W(CO)_4(Ph_2PC_2H_4PPh_2)$ (**1**) with a mercury-arc lamp (cutoff < 350 nm) at room temperature produced the corresponding complex **2a** (Scheme 1). The reaction process was traced by high performance liquid chromatography (HPLC) and the corresponding profiles are shown in Fig. 1a. After irradiation for three minutes, a new peak at 5.9 min was observed in addition to the peaks of the precursors (**1** and Eu@$C_2(5)$-C_{82}), indicative of high regioselectivity. The same procedures conducted on Eu@$C_2(13)$-C_{84} also showed high regioselectivity and presented a single new peak at 6.1 min (Fig. 1b). Subsequent HPLC separations afforded only one product for each EMF (**2a** for Eu@$C_2(5)$-C_{82} and **2b** for Eu@$C_2(13)$-C_{84}). The conversion yields of **2a** and **2b** are estimated to be 51% and 49% according to the HPLC peak areas, respectively.

The electronic structures of the two EMFs have been altered dramatically by the attachment of the tungsten addend, as evidenced by their absorption spectra (Fig. 2a). Since the absorptions of fullerenes and their derivatives are dominated by the $\pi \rightarrow \pi^*$ excitation of the cage π-systems,[2] the changes in absorptions can be ascribed to the charge donation from the exohedral tungsten units onto the fullerene cages. Consistently, our theoretical natural population analysis (NPA) suggests that the fullerene moieties in **2a** and **2b** both receive a negative charge of $-0.35e$ from tungsten. Surprisingly, the two pristine EMFs together with **2a** and **2b** in CS_2 solution show strong photoluminescence (PL) emission. Upon excitation at 406 nm at

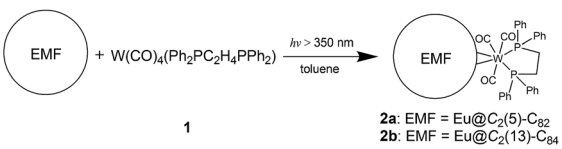

Scheme 1 Reaction of **1** with Eu@$C_2(5)$-C_{82} or Eu@$C_2(13)$-C_{84}.

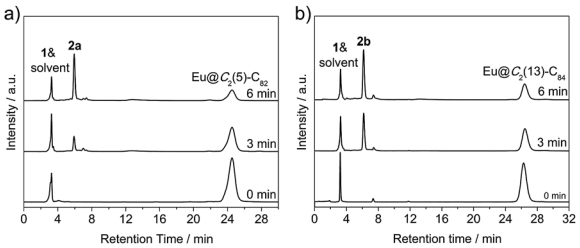

Fig. 1 HPLC profiles of the reaction mixture containing **1** and (a) Eu@$C_2(5)$-C_{82} or (b) Eu@$C_2(13)$-C_{84} probed at different reaction times. HPLC conditions: Buckyprep column (φ = 4.6 × 250 mm); 20 μL injection volume; 1.0 mL min^{-1} toluene flow; 40 °C; 330 nm detection wavelength.

room temperature, two obvious emission bands at *ca.* 450 and 475 nm are generally observed for all four compounds (Fig. 2b). This phenomenon is quite interesting and the origin is currently under investigation in our lab.

Motional control of the internal metal ion by external complexation

The molecular structures of **2a** and **2b** together with those of pristine Eu@$C_2(5)$-C_{82} and Eu@$C_2(13)$-C_{84} co-crystalized with Ni(OEP) (OEP is the dianion of octaethylporphyrin) are unambiguously established by single crystal X-ray crystallography.

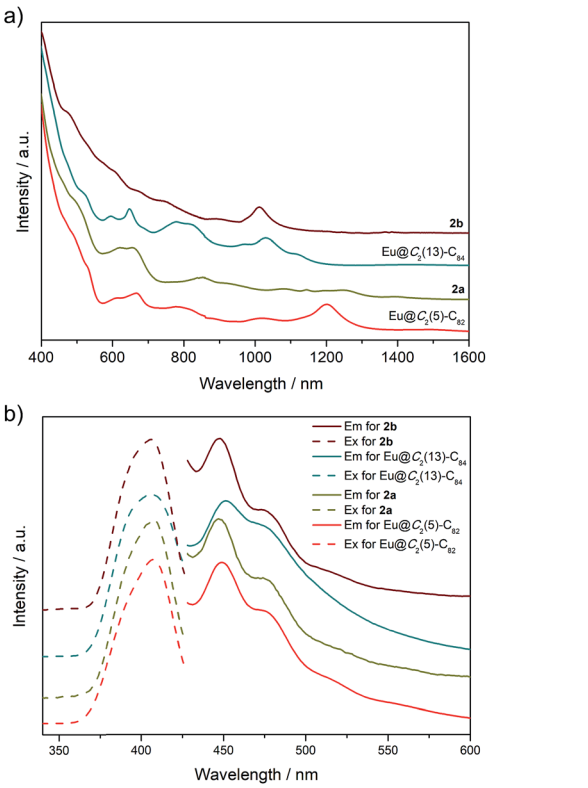

Fig. 2 (a) Vis-NIR absorption spectra and (b) photoluminescence emission and excitation spectra of Eu@$C_2(5)$-C_{82}, **2a**, Eu@$C_2(13)$-C_{84} and **2b** dissolved in CS_2 at room temperature. The curves are vertically shifted for ease of comparison.

The results show an obvious impact of the exohedral complexation on the motional behavior of the internal Eu atom.

The X-ray structures of Eu@C_2(5)-C_{82}/Ni(OEP) are depicted in Fig. 3a. The fullerene cage is unambiguously assigned as C_2(5)-C_{82}. Inside the cage, five disordered Eu sites are distinguished with occupancy values ranging from 0.17 to 0.23, indicative of a moving metal atom. In particular, three Eu sites with a total occupancy of 0.64, including the major one (Eu1, occupancy: 0.23), stay under a hexagonal ring away from the C_2 axis (highlighted with a red circle in Fig. 3a).

In **2a**, the tungsten moiety coordinates to a [6,6]-bond in an η^2-fashion (Fig. 3b and Fig. S1†). The carbon atoms at the sites of addition (C1 and C2) are pulled out from the cage. Their pyramidalization angles[17] increase from 10.65° and 10.66° in the pristine EMF to 15.10° and 15.99° in **2a**, respectively (Table S1†). The C1–C2 bond is coplanar with the two W–P bonds and is elongated from 1.36(2) Å in Eu@C_2(5)-C_{82} to 1.478(6) Å in **2a**, demonstrating substantial back-donation from tungsten to the π*-orbital of the C1–C2 bond.[18] Besides, π–π interaction is found between one of the exohedral phenyl rings and the cage with a plane-to-cage distance of 3.301 Å (Fig. S1†). It is noteworthy that **2a** represents the first example of a functionalized C_2(5)-C_{82} cage, though functionalizations on other C_{82} cages including C_s(6)-C_{82}, C_{3v}(7)-C_{82}, C_{3v}(8)-C_{82} and C_{2v}(9)-C_{82} have been reported.[2,19]

Inside the cage of **2a**, four disordered Eu positions with occupancy values ranging from 0.14 to 0.40 are identified and the major Eu site (Eu1) is located under the hexagonal ring perpendicular to the C_2 cage-axis. These disordered sites all locate away from the addition sites, suggesting a repulsive effect of tungsten on europium through the cage. In contrast, the internal metal atom generally stays closer to the addition sites in the carbene derivatives of M@C_{82} (M = Sc, Y, La, and Gd) as a consequence of bond cleavage of the corresponding cages.[20–23] In addition, our theoretical calculations reveal that the electrostatic potential map of $[C_{82}\cdot W(CO)_3(Ph_2PC_2H_4PPh_2)]^{2-}$ (nearly two electrons are transferred from Eu to the cage, see Table S2†) shows a minimum in the position where the major Eu in **2a** stays (Fig. 3d). Moreover, appreciable differences in the electrostatic potentials inside the cages are observed between $[C_{82}\cdot W(CO)_3(Ph_2PC_2H_4PPh_2)]^{2-}$ and $[C_{82}]^{2-}$ (Fig. 3), theoretically corroborating the charge-transfer-induced motional control of the endohedral europium atom by the exohedral tungsten coordination as observed by crystallographic analysis.

The co-crystals of Eu@C_2(13)-C_{84} and Ni(OEP) belong to the monoclinic space group $C2/m$, and as a result two disordered cage orientations with an equal occupancy of 0.50 are presented. The fullerene cage is unambiguously assigned as C_2(13)-C_{84}. Fig. 4a shows the molecular structure of Eu@C_2(13)-C_{84} together with Ni(OEP). Within the cage, 13 disordered Eu sites (occupancy values: 0.02–0.18) are distinguished, with the major Eu position (Eu1, 0.18 occupancy) locating under a hexagonal

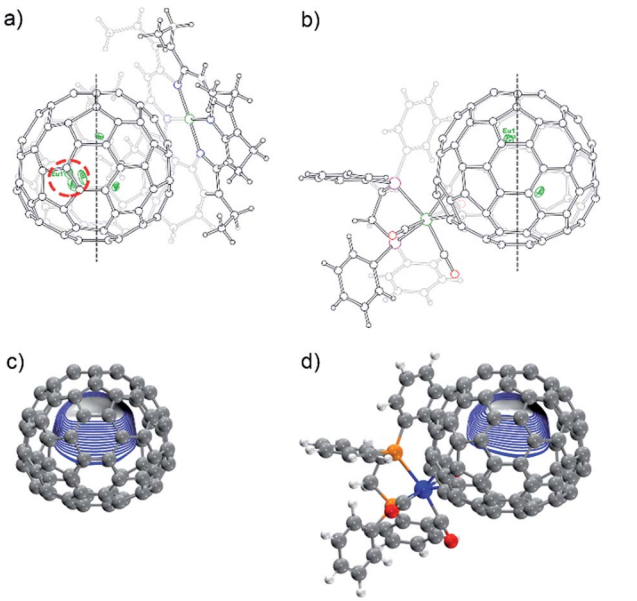

Fig. 3 Molecular structures of (a) Eu@C_2(5)-C_{82}·Ni(OEP) and (b) **2a**. The endohedral Eu atom is depicted with thermal ellipsoids set at the 20% probability level. Only one cage orientation and the major metal site are shown. Solvent molecules and the minor metal sites are omitted for clarity. The prohibited area inside the cage upon exohedral functionalization is highlighted with a red dashed circle. The C_2 axis of the cage is indicated with a black dashed line. The electrostatic potential maps of (c) $[C_2(5)\text{-}C_{82}]^{2-}$ and (d) $[C_2(5)\text{-}C_{82}W(CO)_3(Ph_2PC_2H_4PPh_2)]^{2-}$.

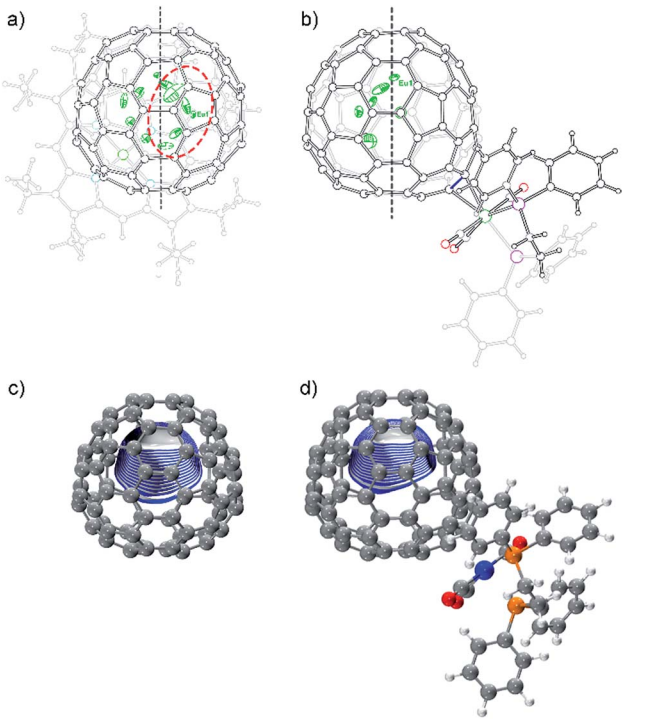

Fig. 4 Molecular structures of (a) Eu@C_2(13)-C_{84}·Ni(OEP) and (b) **2b**. The endohedral Eu ions are depicted with thermal ellipsoids set at the 20% probability level. Only one cage orientation and the major metal sites are shown with solvent molecules and the minor metal sites omitted for clarity. The prohibited area inside the cage upon exohedral functionalization is highlighted with a red dashed circle. The C_2 axis of the C_2(13)-C_{84} cage is marked with a black dashed line. The electrostatic potential maps of (c) $[C_2(13)\text{-}C_{84}]^{2-}$ and (d) $[C_2(13)\text{-}C_{84}W(CO)_3(Ph_2PC_2H_4PPh_2)]^{2-}$.

ring away from the C_2 axis. The disordered phenomenon suggests moving nature of the endohedral europium atom.

In **2b**, the tungsten moiety adds onto a [6,6]-bond in an η^2-fashion to afford a closed structure (Fig. 4b and Fig. S2†), which is different from the [5,6]-fulleroid structure of the reported carbene adduct of Yb@C_2(13)-C_{84} (ref. 24) bearing the same C_2(13)-C_{84} cage, suggesting different reaction mechanisms. The exohedral functionalization has induced a geometric change in the cage. In detail, the pyramidalization angles of the cage carbons at the sites of addition (C1 and C2) are amplified (from 11.44° and 9.31° to 15.40° and 16.83° for C1 and C2, respectively), and the C1–C2 bond length is elongated from 1.38(2) Å in parent Eu@C_2(13)-C_{84} to 1.49(1) Å in **2b** (Table S1†), indicative of remarkable back-donation from tungsten onto the π*-orbital of the C1–C2 bond. Besides, π–π interaction is found between one of the exohedral phenyl rings and the C_2(13)-C_{84} cage with a plane-to-cage distance of 3.306 Å (Fig. S2†).

Within the cage of **2b**, the number of disordered europium sites is reduced to only six (occupancy values: 0.36–0.05). They locate at an area far away from the addition sites with the major position Eu1 staying under a hexagonal ring perpendicular to the C_2 axis of the cage (Fig. 4b). The crystallographic results confirm that the motional behavior of the internal Eu ion has been constrained by the external tungsten addition. Consistently, our calculations suggest that such a motional control is a consequence of the alteration of the electrostatic potential inside the cage upon exohedral coordination (Fig. 4).

Regiochemical control of exohedral addition by internal metal doping

DFT calculations are carried out to explore the origin of the high regioselectivity observed here. Due to the two electron-transfer from Eu onto the cage (Table S2†) and the moving state of the Eu ion in Eu@C_2(5)-C_{82}/Eu@C_2(13)-C_{84}, it is reasonable to consider $[C_2(5)\text{-}C_{82}]^{2-}$ and $[C_2(13)\text{-}C_{84}]^{2-}$ as the prototypes. The coordination reactions of alkenes[18] and C_{60}[25,26] with metallic complexes can be well understood by considering the frontier orbitals where the LUMO of alkenes/C_{60} accepts electrons from metallic complexes to form coordination bonds. Accordingly, the LUMO distributions of $[C_2(5)\text{-}C_{82}]^{2-}$ and $[C_2(13)\text{-}C_{84}]^{2-}$ along with the HOMO distribution of the tungsten addend are calculated (Fig. 5). Clearly, the LUMOs at the C1–C2 bonds on both $[C_2(5)\text{-}C_{82}]^{2-}$ and $[C_2(13)\text{-}C_{84}]^{2-}$ possess pronounced lobes and overlap with the HOMOs of the tungsten addend (mainly the 5d orbital of the tungsten center), implying that the C1–C2 sites are suitable for tungsten addition.

Although LUMO distributions can describe the high regioselectivity in a qualitative way, it is hard to accurately explain the formation of merely one adduct for each EMF (**2a** and **2b**) since as many as 62/63 different types of nonequivalent C–C bonds exist in the C_2(5)-C_{82}/C_2(13)-C_{84} cages, respectively (Fig. S3†). Accordingly, another factor, POAV (p-orbital axis vector) which represents the local strain on the cage carbon atoms[17] is introduced to rationalize the reaction mechanism herein because it has shown great success in elucidating the chemical reactivities of EMFs.[2,17,19] For the ease of comparison, the average LUMO

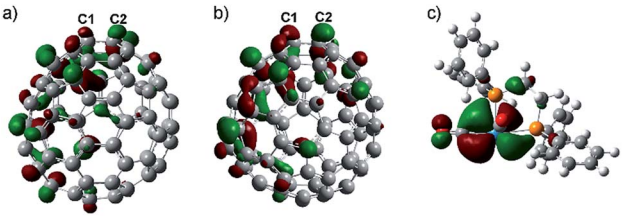

Fig. 5 LUMO distributions of (a) $[C_2(5)\text{-}C_{82}]^{2-}$ and (b) $[C_2(13)\text{-}C_{84}]^{2-}$ and (c) HOMO distributions of the tungsten addend.

and POAV values of the two bonded cage carbons for each type of C–C bond are calculated and presented in Fig. 6. The C1–C2 bond in $[C_2(5)\text{-}C_{82}]^{2-}$ features both pronounced LUMO coefficients and high pyramidal angles, and therefore it is made favorable to accept the electron from the tungsten center to form the coordination bonds with negligible steric hindrance. Similarly, the C1–C2 bond on $[C_2(13)\text{-}C_{84}]^{2-}$ is also preferred owing to its high POAV and LUMO values. The above discussions suggest a synergistic effect of both the electron distribution and geometric structure of the cages on the addition patterns.

In fact, our calculations reveal that the two-electron transfer does not alter the POAV values of the cage atoms but changes the LUMO distributions dramatically for both C_2(5)-C_{82} and C_2(13)-C_{84} (Fig. S4†). In particular, the LUMO distributions at the addition sites (C1–C2 in Fig. S4 and S5†) are remarkably enhanced by Eu-encapsulation with the values increasing from 0.58% to 2.95% for C_2(5)-C_{82} and from 0.15% to 4.97% for C_2(13)-C_{84}, which eventually governs the high regioselectivity observed in the reactions. Accordingly, the addition pattern in **2a** and **2b** and the high regioselectivity in the reactions are controlled by the endohedral metal doping by changing the electronic structures of the corresponding hollow cages.

Another remarkable feature of the reactions is the formation of merely mono-adducts, whilst the reactions of EMFs usually

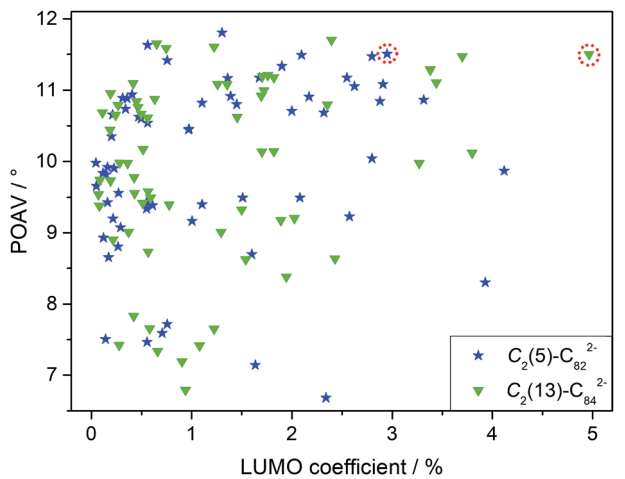

Fig. 6 The average LUMO coefficients and the π-orbital axis vector (POAV) angles of two bonded cage carbons on $[C_2(5)\text{-}C_{82}]^{2-}$ and $[C_2(13)\text{-}C_{84}]^{2-}$. The bonds at the sites of coordination are marked with a red dotted circle. Equivalent C–C bonds on the cages are omitted for clarity.

produced mixtures containing mono-, bis- and multi-adducts.[2,19,27,28] According to the reaction mechanism stated above, the LUMO and POAV distributions of the **2a** and **2b** were calculated (Fig. S6†). It is clear that the sites featuring both large POAV values and pronounced LUMO distributions are all close to the existing tungsten addend. Accordingly, further additions are prevented by the steric hindrance of the bulky tungsten addend. Thus, this work presents a practical strategy for the controlled synthesis of EMF-derivatives in a highly regioselective manner.

Conclusions

Reacting a tungsten complex $W(CO)_4(Ph_2PC_2H_4PPh_2)$ (**1**) with either Eu@C_2(5)-C_{82} or Eu@C_2(13)-C_{84} affords a sole mono-adduct for each metallofullerene (**2a** for Eu@C_2(5)-C_{82} and **2b** for Eu@C_2(13)-C_{84}). The X-ray results of **2a**, **2b** and the two pristine EMFs cocrystallized with Ni(OEP) clearly show that the motional behavior of the Eu atom inside the cage is significantly restricted upon exohedral tungsten addition, as a result of electrostatic potential redistribution. Meanwhile, theoretical results demonstrate that the endohedral Eu-doping has changed the LUMO distributions on the cages *via* charge transfer, which eventually leads to the regioselective addition of the exohedral tungsten addend. It is now evident that it is possible for the endohedral and exohedral metallic units in the complexes of EMFs to interact with each other *via* intramolecular charge transfer, highlighting the potential for the synthesis of EMF-based molecular devices with novel magnetic or electronic properties.

Experimental

$W(CO)_4(Ph_2PC_2H_4PPh_2)$ (**1**) was synthesized according to the procedures described in the literature.[29] Eu@C_2(5)-C_{82} and Eu@C_2(13)-C_{84} were produced with an arc-discharge method and were isolated with multi-stage HPLC (Fig. S7†).[30] The reaction between **1** and Eu@C_2(5)-C_{82}/Eu@C_2(13)-C_{84} was monitored with an HPLC system (LC-16, SHIMADZU LIMITED) equipped with an analytical Buckyprep column (∅ 4.6 × 250 mm). The separation was conducted on an HPLC machine (LC-908; Japan Analytical Industry Co. Ltd.) equipped with a preparative Buckyprep column (∅ 20 × 250 mm) with toluene as the eluent. The Vis-NIR experiments were carried out on a PE Lambda 750S UV-vis-NIR spectrophotometer and photoluminescence spectra were recorded on a Jasco FP-6500 machine.

Crystallographic characterization

Single-crystal X-ray data were collected at 100 K using a radiation wavelength of 0.65250 Å with a MarCCD detector at beamline BL17B of the Shanghai Synchrotron Radiation Facility (China). A multi-scan method (SADABS) was used for absorption corrections. The structures were solved with direct methods and were refined with SHELXL-2016.[31] Cocrystals of Eu@C_2(5)-C_{82} or Eu@C_2(13)-C_{84} were obtained by slow diffusion of a benzene solution of Ni^{II}(OEP) (OEP = octaethylporphyrin) into a CS_2 solution of the respective EMF in a glass tube at room temperature for four weeks. Crystals of **2a** or **2b** were obtained by slow diffusion of *n*-hexane into a CS_2 solution of **2a** or **2b** in glass tubes at room temperature for two weeks, respectively.

Theoretical calculations

Density functional theory calculations were carried out by using the M06-2X functional in conjunction with the SDD basis set and the corresponding effective core potential for W and Eu and the standard 6-31G* basis set for all other atoms (denoted as 6-31G*∼SDD) as implemented in the Gaussian 09 software package.[32–35] A spin multiplicity of $M = 8$ was employed according to the half-filled 4f shell of the Eu^{2+} ion.

Chemical functionalization of Eu@C_2(5)-C_{82}/Eu@C_2(13)-C_{84}

In a typical reaction, a toluene solution containing *ca.* 2 mg (1.8 μmol) of Eu@C_2(5)-C_{82} and 24 mg (34.6 μmol) of **1** was degassed with the freeze–pump–thaw method for three cycles. The mixture was then photo-irradiated with a mercury-arc lamp (cutoff < 350 nm) at room temperature for six minutes. The reaction mixture was concentrated and subjected to HPLC separations to afford **2a**. The same procedures performed on Eu@C_2(13)-C_{84} produced **2b**.

Conflicts of interest

There are no conflicts to declare.

Acknowledgements

Financial support from the NSFC (Grants 51672093, 51602112 and 51602097) is gratefully acknowledged. We thank the staff from the BL17B beamline of the National Center for Protein Sciences Shanghai at the Shanghai Synchrotron Radiation Facility, for assistance during data collection, and the Analytical and Testing Center in the Huazhong University of Science and Technology for all related measurements.

Notes and references

1 N. S. Sariciftci, L. Smilowitz, A. J. Heeger and F. Wudl, *Science*, 1992, **258**, 1474–1476.
2 A. Popov, S. Yang and L. Dunsch, *Chem. Rev.*, 2013, **113**, 5989–6113.
3 X. Lu, L. Echegoyen, A. L. Balch, S. Nagase and T. Akasaka, *Endohedral Metallofullerenes: Basics and Applications*, CRC Press, 2014.
4 R. D. Bolskar, A. F. Benedetto, L. O. Husebo, R. E. Price, E. F. Jackson, S. Wallace, L. J. Wilson and J. M. Alford, *J. Am. Chem. Soc.*, 2003, **125**, 5471–5478.
5 B. C. Thompson and J. M. J. Fréchet, *Angew. Chem., Int. Ed.*, 2008, **47**, 58–77.
6 S. Yang, T. Wei and F. Jin, *Chem. Soc. Rev.*, 2017, **46**, 5005–5058.
7 M. Yamada, Y. Tanabe, J.-S. Dang, S. Sato, N. Mizorogi, M. Hachiya, M. Suzuki, T. Abe, H. Kurihara, Y. Maeda,

X. Zhao, Y. Lian, S. Nagase and T. Akasaka, *J. Am. Chem. Soc.*, 2016, **138**, 16523–16532.
8 T. Cai, Z. X. Ge, E. B. Iezzi, T. E. Glass, K. Harich, H. W. Gibson and H. C. Dorn, *Chem. Commun.*, 2005, 3594–3596.
9 C. M. Cardona, A. Kitaygorodskiy and L. Echegoyen, *J. Am. Chem. Soc.*, 2005, **127**, 10448–10453.
10 C. M. Cardona, B. Elliott and L. Echegoyen, *J. Am. Chem. Soc.*, 2006, **128**, 6480–6485.
11 N. Chen, E. Y. Zhang, K. Tan, C. R. Wang and X. Lu, *Org. Lett.*, 2007, **9**, 2011–2013.
12 M. Yamada, T. Akasaka and S. Nagase, *Acc. Chem. Res.*, 2010, **43**, 92–102.
13 H. Fang, H. Cong, M. Suzuki, L. Bao, B. Yu, Y. Xie, N. Mizorogi, M. M. Olmstead, A. L. Balch, S. Nagase, T. Akasaka and X. Lu, *J. Am. Chem. Soc.*, 2014, **136**, 10534–10540.
14 B. Wu, T. Wang, Y. Feng, Z. Zhang, L. Jiang and C. Wang, *Nat. Commun.*, 2015, **6**, 6468.
15 N. B. Shustova, Y. S. Chen, M. A. Mackey, C. E. Coumbe, J. P. Phillips, S. Stevenson, A. A. Popov, O. V. Boltalina and S. H. Strauss, *J. Am. Chem. Soc.*, 2009, **131**, 17630–17637.
16 F. Jin, S. Wang, N. B. Tamm, S. Yang and S. I. Troyanov, *Angew. Chem., Int. Ed.*, 2017, **56**, 11990–11994.
17 R. C. Haddon, *Science*, 1993, **261**, 1545–1550.
18 A. Ariafard, *J. Organomet. Chem.*, 2004, **689**, 2275–2283.
19 X. Lu, L. Feng, T. Akasaka and S. Nagase, *Chem. Soc. Rev.*, 2012, **41**, 7723–7760.
20 Y. Maeda, Y. Matsunaga, T. Wakahara, S. Takahashi, T. Tsuchiya, M. O. Ishitsuka, T. Hasegawa, T. Akasaka, M. T. H. Liu, K. Kokura, E. Horn, K. Yoza, T. Kato, S. Okubo, K. Kobayashi, S. Nagase and K. Yamamoto, *J. Am. Chem. Soc.*, 2004, **126**, 6858–6859.
21 T. Akasaka, T. Kono, Y. Takematsu, H. Nikawa, T. Nakahodo, T. Wakahara, M. O. Ishitsuka, T. Tsuchiya, Y. Maeda, M. T. H. Liu, K. Yoza, T. Kato, K. Yamamoto, N. Mizorogi, Z. Slanina and S. Nagase, *J. Am. Chem. Soc.*, 2008, **130**, 12840–12841.
22 X. Lu, H. Nikawa, L. Feng, T. Tsuchiya, Y. Maeda, T. Akasaka, N. Mizorogi, Z. Slanina and S. Nagase, *J. Am. Chem. Soc.*, 2009, **131**, 12066–12067.
23 M. Hachiya, H. Nikawa, N. Mizorogi, T. Tsuchiya, X. Lu and T. Akasaka, *J. Am. Chem. Soc.*, 2012, **134**, 15550–15555.
24 W. Zhang, M. Suzuki, Y. Xie, L. Bao, W. Cai, Z. Slanina, S. Nagase, M. Xu, T. Akasaka and X. Lu, *J. Am. Chem. Soc.*, 2013, **135**, 12730–12735.
25 J. A. López and C. Mealli, *J. Organomet. Chem.*, 1994, **478**, 161–171.
26 H. Zheng, X. Zhao and S. Sakaki, *Inorg. Chem.*, 2017, **56**, 6746–6754.
27 W. Zhang, M. Suzuki, Y. Xie, L. Bao, W. Cai, Z. Slanina, S. Nagase, M. Xu, T. Akasaka and X. Lu, *J. Am. Chem. Soc.*, 2013, **135**, 12730–12735.
28 Y. P. Xie, M. Suzuki, W. Cai, N. Mizorogi, S. Nagase, T. Akasaka and X. Lu, *Angew. Chem., Int. Ed.*, 2013, **52**, 5142–5145.
29 S. O. Grim, W. L. Briggs, R. C. Barth, C. A. Tolman and J. P. Jesson, *Inorg. Chem.*, 1974, **13**, 1095–1100.
30 L. Bao, P. Yu, C. Pan, W. Shen and X. Lu, *Chem. Sci.*, 2019, **10**, 2153–2158.
31 G. M. Sheldrick, *Acta Crystallogr., Sect. A: Found. Crystallogr.*, 2008, **64**, 112–122.
32 M. J. Frisch, G. W. Trucks, H. B. Schlegel, G. E. Scuseria, M. A. Robb, J. R. Cheeseman, G. Scalmani, V. Barone, B. Mennucci, G. A. Petersson, H. Nakatsuji, M. Caricato, X. Li, H. P. Hratchian, A. F. Izmaylov, J. Bloino, G. Zheng, J. L. Sonnenberg, M. Hada, M. Ehara, K. Toyota, R. Fukuda, J. Hasegawa, M. Ishida, T. Nakajima, Y. Honda, O. Kitao, H. Nakai, T. Vreven, J. A. Montgomery Jr., J. E. Peralta, F. Ogliaro, M. J. Bearpark, J. Heyd, E. N. Brothers, K. N. Kudin, V. N. Staroverov, R. Kobayashi, J. Normand, K. Raghavachari, A. P. Rendell, J. C. Burant, S. S. Iyengar, J. Tomasi, M. Cossi, N. Rega, N. J. Millam, M. Klene, J. E. Knox, J. B. Cross, V. Bakken, C. Adamo, J. Jaramillo, R. Gomperts, R. E. Stratmann, O. Yazyev, A. J. Austin, R. Cammi, C. Pomelli, J. W. Ochterski, R. L. Martin, K. Morokuma, V. G. Zakrzewski, G. A. Voth, P. Salvador, J. J. Dannenberg, S. Dapprich, A. D. Daniels, Ö. Farkas, J. B. Foresman, J. V. Ortiz, J. Cioslowski and D. J. Fox, *Gaussian 09*, Gaussian, Inc., Wallingford, CT, USA, 2009.
33 Y. Zhao and D. G. Truhlar, *Theor. Chem. Acc.*, 2008, **120**, 215–241.
34 W. J. Hehre, R. Ditchfield and J. A. Pople, *J. Chem. Phys.*, 1972, **56**, 2257–2261.
35 P. J. Hay and W. R. Wadt, *J. Chem. Phys.*, 1985, **82**, 299–310.